Paleoceanography and Paleoclimatology

RESEARCH ARTICLE
10.1029/2018PA003503

Special Section:
Climatic and Biotic Events of the Paleogene: Earth Systems and Planetary Boundaries in a Greenhouse World

Atlantic Deep-Sea Cherts Associated With Eocene Hyperthermal Events

Donald E. Penman[1], Allison Keller[2], Simon D'haenens[1], Sandra Kirtland Turner[2], and Pincelli M. Hull[1]

[1]Department of Geology and Geophysics, Yale University, New Haven, CT, USA, [2]Department of Earth Science, University of California, Riverside, CA, USA

Key Points:
- Chert and porcelainite are exceptionally common in the Atlantic during the Eocene, a warm period punctuated by numerous discrete hyperthermal events
- New stable isotope records demonstrate that many of these Eocene Atlantic siliceous horizons correlate to hyperthermal events, including a new record of the Paleocene-Eocene Thermal Maximum
- Geochemical modeling demonstrates that both the global silicate weathering response to hyperthermals and deep-ocean circulation change are important in the formation of Eocene Atlantic hyperthermal-associated cherts

Supporting Information:
- Supporting Information S1
- Data Set S1
- Data Set S2

Correspondence to:
D. E. Penman,
donald.penman@yale.edu

Citation:
Penman, D. E., Keller, A., D'haenens, S., Kirtland Turner, S., & Hull, P. M. (2019). Atlantic deep-sea cherts associated with Eocene hyperthermal events. *Paleoceanography and Paleoclimatology*, *34*. https://doi.org/10.1029/2018PA003503

Received 24 OCT 2018
Accepted 28 JAN 2019
Accepted article online 30 JAN 2019

Abstract Chert, porcelainite, and other siliceous phases are exceptionally common in Atlantic sedimentary records of the early Eocene, but the origins of these facies remain enigmatic. The early Eocene was also the warmest interval of the entire Cenozoic Era, punctuated by numerous discrete warming events termed "hyperthermals," the largest of which is termed the Paleocene-Eocene Thermal Maximum (~56 Ma). Here we present new and published lithologic and carbon isotope records of silica-bearing lower Eocene sediments and suggest a link between the ubiquitous Atlantic cherts of that time period and hyperthermal events. Our data demonstrate that many of these Atlantic siliceous horizons coincide with negative carbon isotope excursions (a hallmark of hyperthermal events), including a previously unrecognized record of the Paleocene-Eocene Thermal Maximum in the South Atlantic. Hyperthermal-associated silica burial appears to be focused in the western middle to high latitudes of both the North and South Atlantic, with no association between siliceous facies and hyperthermal events found in the Pacific. We also present a new model of the coupled carbon and silica cycles (LOSiCAR) to demonstrate that enhanced silicate weathering during these events would require a rapid increase in total marine silica burial. Model experiments that include previously suggested transient reversals in the pattern of deep-ocean circulation during hyperthermals demonstrate that such a mechanism can explain the apparent focusing of elevated silica burial into the Atlantic. This combination—a silicate weathering feedback in response to global warming along with a circulation-driven focusing of silica burial—represents a new mechanism for the formation of deep-sea cherts in lower Eocene Atlantic sedimentary records and may be relevant to understanding chert formation in other intervals of Earth history.

1. Introduction

Since as early as Deep Sea Drilling Project Leg 1, silica-rich sedimentary layers in the form of porcelainite (containing SiO_2 as opal and its intermediate diagenetic products cristobalite and tridymite) and chert (consisting of microcrystalline quartz) have been encountered in Atlantic pelagic sediments of Eocene age (Figure 1)—often inhibiting complete core recovery (Calvert, 1971). The origin of these siliceous layers is debated, with proposed formation mechanisms including the alteration of radiolarian/diatom oozes (Hesse, 1988), alteration of volcanic glass from ash falls (Gibson & Towe, 1971), direct inorganic precipitation of precursor phases from seawater (Laschet, 1984; Muttoni & Kent, 2007), a response to changes in global silicate weathering rates on geologic timescales ($>10^6$ years; Muttoni & Kent, 2007), complex scenarios of submarine volcanism coupled to climatic and ocean circulation change (McGowran, 1989), or combinations of the above. Other chert formation mechanisms not specifically linked to Atlantic Eocene cherts include dissolution and hydrothermal reprecipitation of silica from basal oceanic basalt (Moore, 2008) and the mixing of meteoric groundwater and marine pore water as a means to elevate silica saturation states (Knauth, 1979).

In recent decades, multiple high-resolution paleoceanographic records have revealed that early Eocene climate was repeatedly perturbed by transient warming events termed "hyperthermals" (Kirtland Turner et al., 2014; Sexton et al., 2011; Zachos et al., 2010) characterized by global warming (Dunkley-Jones et al., 2013; Zachos et al., 2003), ocean acidification (Babila et al., 2018; Penman et al., 2014; Zachos et al., 2005), and global negative carbon isotope excursions (CIEs; Alley, 2016; Kennett & Stott, 1991; Koch et al., 1992). These events range in size from the Paleocene-Eocene Thermal Maximum (PETM, ~56 Ma, a >2 permil (‰) CIE lasting ~150,000 years; McInerney & Wing, 2011) to smaller (<1‰ CIE) orbitally paced events occurring semiperiodically throughout the early Eocene Climatic Optimum (50–53 Ma) (Kirtland Turner et al., 2014;

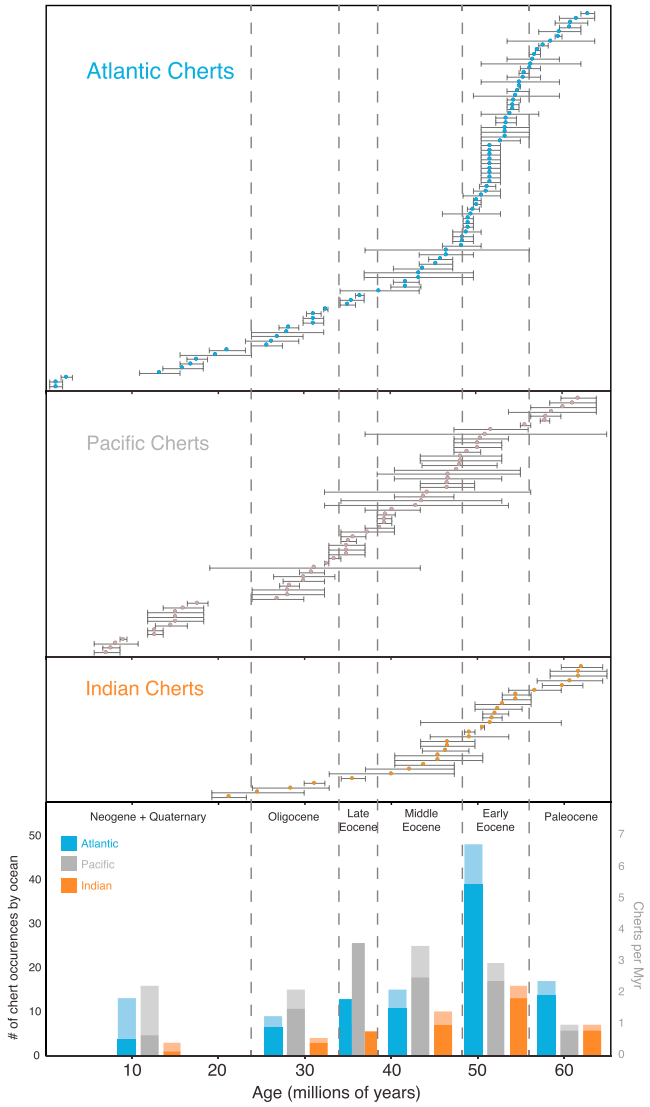

Figure 1. Chert occurrences in DSDP/ODP/IODP drill sites, separated by ocean basin, demonstrating the exceptionally high concentration of lower Eocene cherts in the Atlantic. Occurrences are from the compilation of Muttoni and Kent (2007), updated with recent cherts from IODP drilling. In the upper three panels, each point represents a stratigraphic interval (with horizontal bars showing the beginning and end of each cherty interval) at a single DSDP/ODP/IODP site which may contain several chert horizons. The data are subject to the sampling bias imposed by selective drilling that targets sediments of interest, which is not evenly or randomly distributed through space and time. However, as pointed out by Muttoni and Kent (2007), this cannot be not responsible for overall trends in chert occurrence over time (as the trends persist even when corrected for the chronostratigraphic coverage of all DSDP/ODP holes). Furthermore, if any Atlantic-specific drilling bias was responsible for the peak in lower Eocene Atlantic cherts, we would expect that to persist throughout the Cenozoic; on the contrary, more Pacific cherts were encountered for all periods younger than the early Eocene. The histogram of chert occurrences includes raw counts of chert intervals (solid bars) and chert occurrences normalized by the length of each interval (number of cherts per interval divided by interval duration, in units of cherts per million years, grayed out bars). DSDP = Deep Sea Drilling Project; ODP = Ocean Drilling Program; IODP = Integrated Ocean Drilling Program.

Littler et al., 2014; Sexton et al., 2011; Westerhold et al., 2018). Coupled with evidence for temperature rise (often in the form of coincident negative oxygen isotope excursions) and deep-sea sedimentary carbonate dissolution, hyperthermals are interpreted to be associated with the geologically rapid ($<10^4$ years) release of thousands of gigatons (Gt C) of ^{13}C-depleted carbon into the exogenic carbon cycle (Gutjahr et al., 2017; Panchuk et al., 2008; Penman & Zachos, 2018; Sexton et al., 2011; Zeebe et al., 2009). Modern understanding of the carbon cycle posits that an important negative feedback to such perturbation is the response of silicate weathering to climate: During the warm, high pCO_2 conditions immediately following carbon release, silicate weathering rates are thought to increase, consuming excess atmospheric CO_2 and cooling climate (Berner et al., 1983; Walker et al., 1981). Indeed, carbon cycle modeling scenarios of the PETM and other hyperthermals typically invoke enhanced silicate weathering as the principal negative feedback responsible for driving the recovery and termination of such events (Dickens et al., 1997; Penman et al., 2016; Zeebe et al., 2009), and both sedimentary (Kelly et al., 2010; Penman, 2016; Penman et al., 2016) and geochemical (Dickson et al., 2015; Ravizza et al., 2001) evidence support enhanced silicate weathering in response to warming, at least in the case of the PETM.

Penman (2016) used back-of-the-envelope calculations and a simple two-box model of the marine silica cycle to demonstrate that if silicate weathering were responsible for sequestering the mass of carbon estimated to have been released during PETM, this would have significantly elevated the riverine delivery of dissolved silica to the oceans and required a geologically rapid (within 10^4–10^5 years) increase in sedimentary SiO_2 burial to balance that input flux. New sedimentary records from the North Atlantic (Integrated Ocean Drilling Program [IODP] Sites U1403, U1408, and U1409) that exhibit chert layers and other siliceous facies coincident with the PETM were proposed to be the result of a dramatic increase in terrestrial silicate weathering rates during the global warmth of the PETM. However, the apparently unique nature of the North Atlantic PETM cherts remains puzzling, as there are dozens of documented deep-sea PETM records where increased silica deposition was not previously observed. Similarly, the question of whether the processes responsible for North Atlantic chert deposition during the PETM were unique to that event or whether they operated in response to other hyperthermal events also remains unanswered. So too does the question of whether early Eocene hyperthermal events could together account for the long-recognized peak in chert deposition in lower Eocene Atlantic pelagic sediments (Figure 1).

Here we present new sedimentary records from deep-sea drill sites in the North Atlantic, South Atlantic, Caribbean, and Western Pacific (Figure 2) that contain siliceous facies (siliceous microfossils, silica-cemented clay and chalk, porcelainite, and chert) from the lower Eocene and construct bulk carbonate stable isotope records to investigate the timing of trends in silica burial with respect to Eocene hyperthermal events, including the PETM (Figures 3–7). We explore the resulting trends with a new model of the coupled carbon and marine silica cycles (LOSiCAR, Figures 8 and 9) to evaluate the potential roles of silicate weathering and circulation change in both global and regional changes in silica burial in response to carbon injection during hyperthermal events (Figure 8).

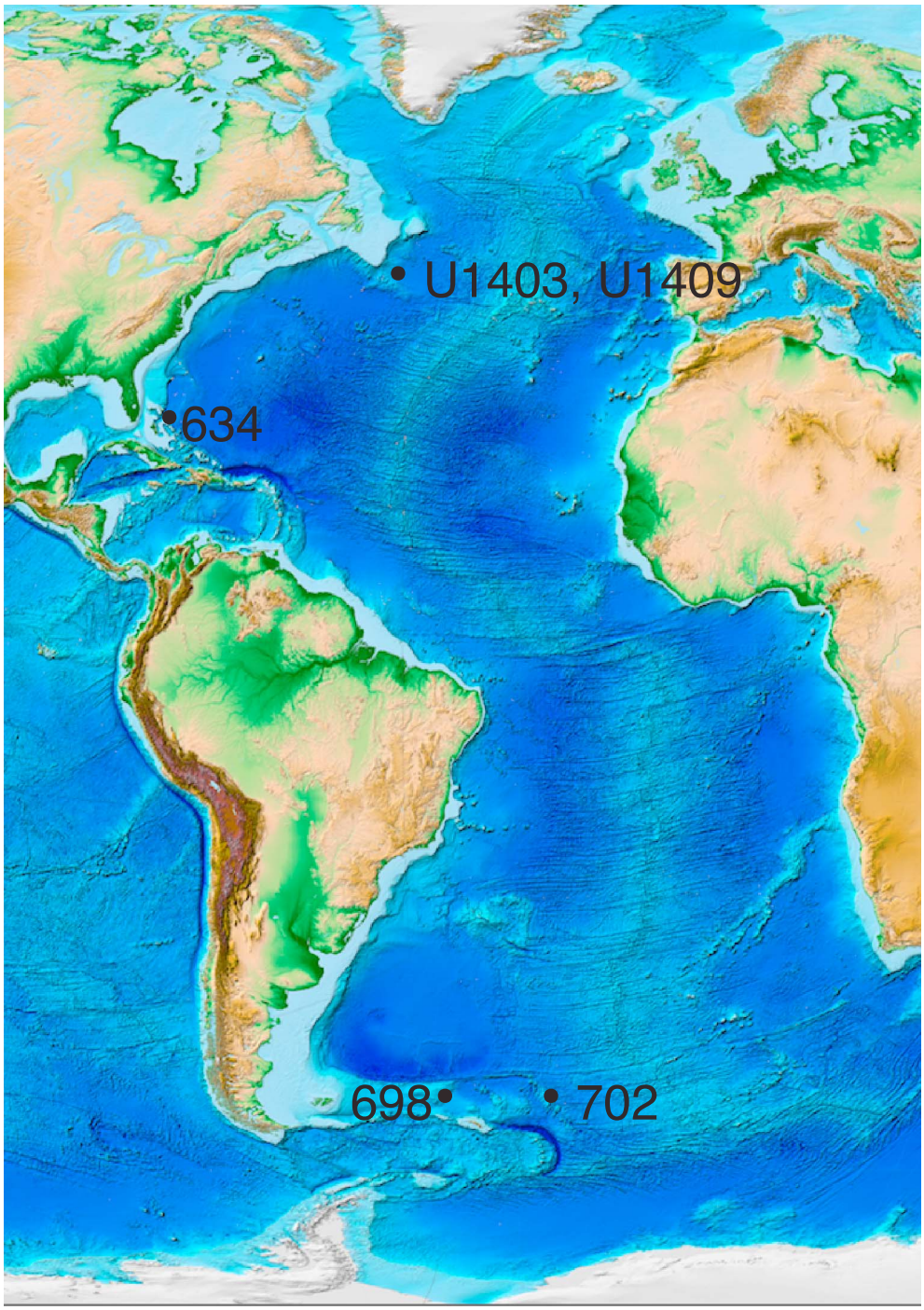

Figure 2. Site map of Atlantic sites bearing hyperthermal-associated siliceous sediments. Not shown is Site 1183, which is on the Ontong-Java Plateau in the western Pacific.

2. New Carbon Isotope Records of Atlantic Eocene Siliceous Sediments

Samples (1–2 cm^3) were taken at 1- to 10-cm resolution (with higher sample density around porcelainite/chert layers) from siliceous and carbonate facies-bearing sediments of early Eocene age at Ocean Drilling Program (ODP) Site 634 (25°23.02′N, 77°18.88′W, 2,835-m water depth) in the Caribbean (Austin et al., 1986) and Site 698 (51°27.51′S, 33°05.96′W, 2,138-m depth) and 702 (50°56.786′S, 26°22.127′W, 3,083-m depth) in the South Atlantic (Ciesielski & Kristoffersen, 1988) and IODP Site U1409 (41°17.75′N,

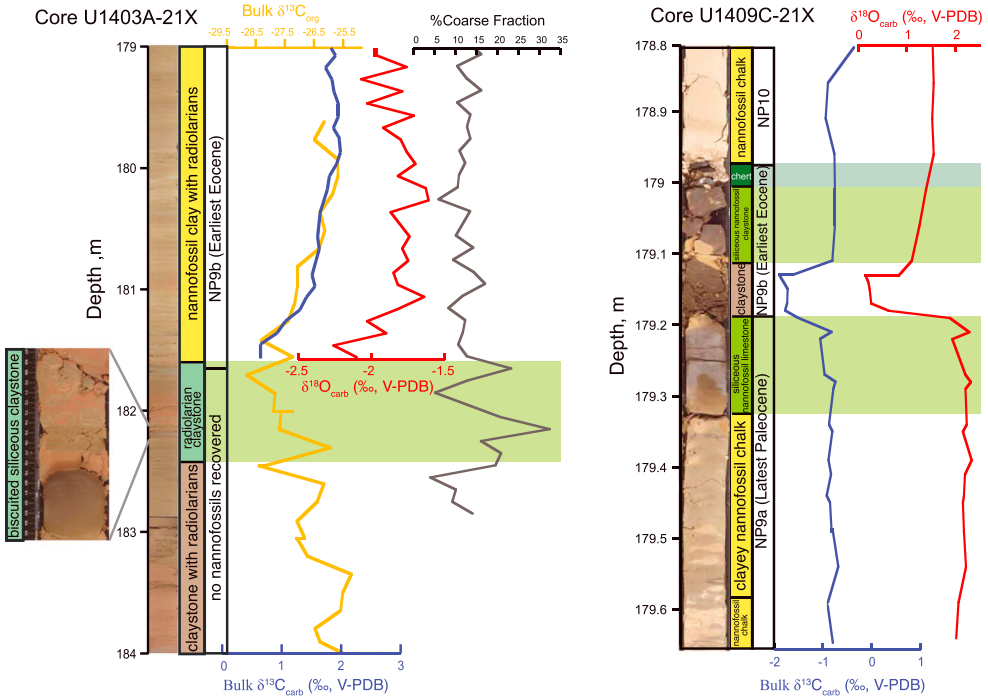

Figure 3. Siliceous sediments spanning the Paleocene-Eocene Thermal Maximum from Expedition 342 (Newfoundland Ridge, North Atlantic; Penman, 2016). Each record consists of a core photo, generalized lithostratigraphy, biostratigraphic constraints, and bulk carbonate stable isotope records ($\delta^{13}C_{carb}$ and $\delta^{18}O_{carb}$). These are supplemented by $\delta^{13}C_{org}$, percent coarse fraction (>63 μm reflecting an increase in radiolarian content), and $\delta^{13}C_{org}$ at Site U1403 (Penman et al., 2016). Green shaded bars represent siliceous facies. V-PDB = Vienna Pee Dee Belemnite.

49°14.00′W, 3,503-m depth) in the North Atlantic (Norris et al., 2014a) and Site 1183 (0°40.7873′S, 159°50.6519′E, 2,729-m depth) on the Ontong-Java Plateau in the western Pacific. Samples were oven dried and homogenized by mortar and pestle, and ~60-μg aliquots of carbonate or up to several milligrams of porcelainite/chert (due to low wt % $CaCO_3$) were analyzed for stable carbon and oxygen isotope ratios ($\delta^{13}C_{carb}$ and $\delta^{18}O_{carb}$) using a ThermoFisher MAT 253 (Yale University) or Delta V (UC-Riverside) stable isotope mass spectrometer, each coupled to a Kiel IV carbonate device using standard carbonate stable isotope techniques. Results are expressed using conventional delta notation, in per mil relative to the Vienna Pee Dee Belemnite standard. The long-term $\delta^{13}C$ and $\delta^{18}O$ reproducibility of carbonate standards are < ±0.05‰, and < ±0.1‰ (1 standard deviation) on both instruments. In addition, the surfaces of Site U1409 cores of interest were scanned at 1- to 2-cm resolution using an Avaatech X-ray fluorescence (XRF) core scanner at the Scripps Institution of Oceanography. Estimates of the total abundance of Si were obtained at an energy level of 10 kV, a current of 500 μA, and a count time of 20 s over a measurement area of 10 × 12 mm. These new records are supplemented by existing data sets from the PETM at Sites U1403 and U1409 (Penman, 2016) in the North Atlantic (Figure 3).

Collectively, we find widespread evidence for an association of siliceous sediments and early Eocene hyperthermal events in the Atlantic Ocean, though not in the Pacific (Figures 3–7). At Site 702 in the subpolar South Atlantic (Figure 4), Core 702B-27X consists of white nannofossil chalk of latest Paleocene nannofossil zone NP9 interrupted by ~30 cm of siliceous chalk containing an ~5-cm-thick brown chert layer (Ciesielski & Kristoffersen, 1988). Coincident with this siliceous unit, we observe an ~2‰ decrease in bulk carbonate $\delta^{13}C$ and an ~1‰ decrease in $\delta^{18}O$ (suggesting 4–5 °C of surface warming, similar to that observed globally for the PETM; Dunkley-Jones et al., 2013). This isotope excursion is followed by a recovery in both records within the overlying ~10 cm. The size and shape of the $\delta^{13}C$ excursion, the extent of warming, and its occurrence within or immediately above the latest Paleocene nannofossil zone NP9 and very near the Paleocene-Eocene benthic faunal turnover (Ciesielski & Kristoffersen, 1988; Katz & Miller, 1991) unambiguously correlate this CIE to the PETM, which was previously unrecognized at Site 702. The sequence of

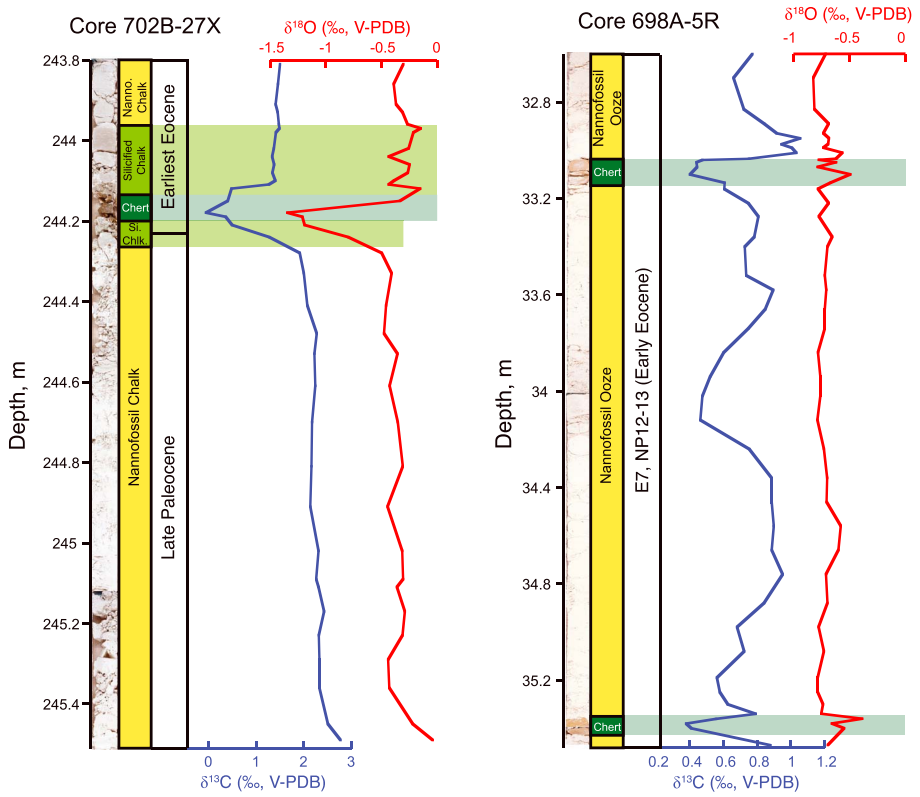

Figure 4. New Records of lower Eocene siliceous sediments from the South Atlantic (Sites 702 and 698). Each record consists of a core photo, generalized lithostratigraphy, biostratigraphic constraints, and bulk carbonate stable isotope records ($\delta^{13}C_{carb}$ and $\delta^{18}O_{carb}$). The large excursion in $\delta^{13}C_{carb}$ and $\delta^{18}O_{carb}$ at Site 702 represents the Paleocene-Eocene Thermal Maximum. V-PDB = Vienna Pee Dee Belemnite.

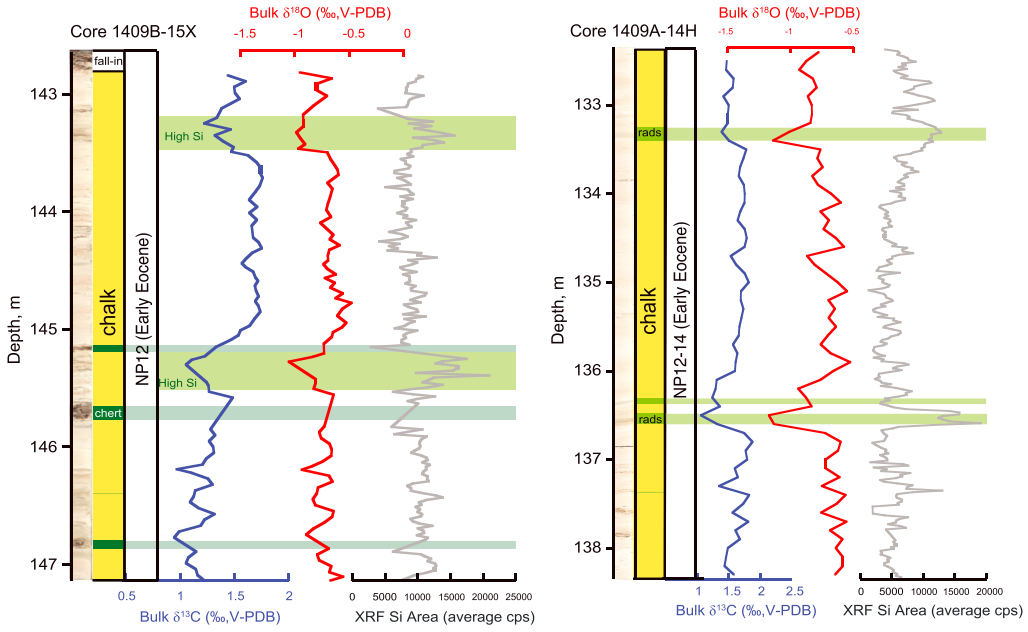

Figure 5. New records of lower Eocene siliceous sediments at Site 1409 (Newfoundland Ridge, North Atlantic). Each record consists of a core photo, generalized lithostratigraphy, biostratigraphic constraints, bulk carbonate stable isotope records ($\delta^{13}C_{carb}$ and $\delta^{18}O_{carb}$), and XRF-derived [Si]. Green shaded bars represent siliceous facies, with intervals of high Si concentration (as demonstrated by XRF) noted. V-PDB = Vienna Pee Dee Belemnite; XRF = X-ray fluorescence.

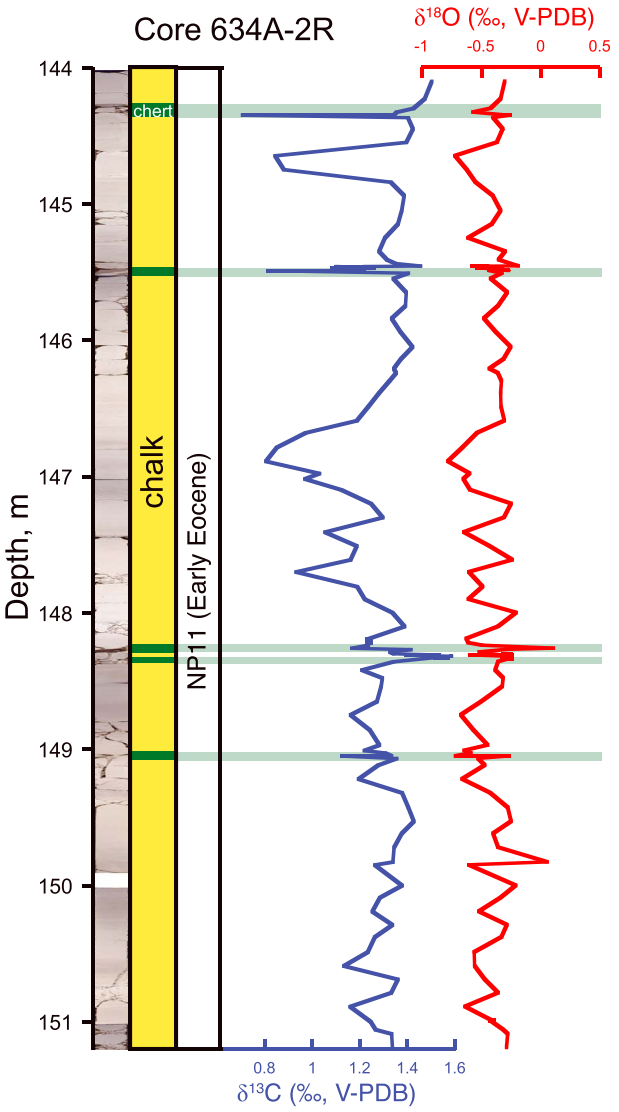

Figure 6. New record of lower Eocene siliceous sediments at Site 634 (Caribbean). Shown are core photo, generalized lithostratigraphy, biostratigraphic constraints, and bulk carbonate stable isotope records ($\delta^{13}C_{carb}$ and $\delta^{18}O_{carb}$). V-PDB = Vienna Pee Dee Belemnite.

siliceous limestone and chert bracketing the PETM at Site 702 bears a resemblance to that observed at Site U1409 in the North Atlantic (Penman, 2016).

At Site U1409, off Newfoundland in the North Atlantic, the occurrence of siliceous sediments at the PETM was previously documented by Penman (2016) (Figure 3) and comprises a sequence of silicified chalk, claystone, and chert coincident with the PETM CIE. However, the overlying lower Eocene chalk at this site is also interrupted by numerous thin chert layers and intervals of elevated radiolarian concentration (Norris et al., 2014a). To test whether these siliceous facies are also associated with hyperthermals, we constructed bulk and benthic stable isotope records over several chert and radiolarian-rich layers (Figure 5). In Core U1409B-15X, lower Eocene nannofossil chalk of nannofossil zone NP12 (~50.4–53.7 Ma) is interrupted by two centimeter-scale chert layers bracketing ~30 cm of sediment with higher SiO_2 content (identifiable as an increase in Si from XRF core-scanning records) at 145.5 m. Across this sequence of siliceous sediments, bulk $\delta^{13}C$ shows a negative excursion of 0.5‰, coincident with warming of 2–3 °C indicated by a negative excursion in $\delta^{18}O$. Higher up in the same core, another interval of elevated Si coincides with similar, albeit smaller, excursions in both $\delta^{13}C$ and $\delta^{18}O$. In Core U1409A-14H, bulk $\delta^{13}C$ shows another two ~0.5‰ negative excursions coincident with intervals of radiolarian-rich nannofossil ooze (Norris et al., 2014a), again supported by increases in [Si] documented by XRF records. These excursions are likely correlative with previously identified hyperthermals during the Early Eocene Climate Optimum (Kirtland Turner et al., 2014).

At Site 698 in the subpolar South Atlantic (Figure 4), the Paleocene-Eocene boundary was penetrated but very poorly recovered, presumably due to extensive silicification as only chert fragments were recovered in the lowermost Eocene core (Ciesielski & Kristoffersen, 1988). However, the overlying lower Eocene sediments were partially recovered and yielded nannofossil chalk from early Eocene nannofossil zones NP12–13 (49.2–53.7 Ma; Gradstein et al., 2012). Core 698A-5R contains white nannofossil chalk interrupted by two discrete ~5-cm-thick layers of mottled pale yellow chert (Ciesielski & Kristoffersen, 1988). Each of these chert layers coincides with an ~0.5‰ negative excursion in our new record of bulk carbonate $\delta^{13}C$, which we interpret as hyperthermal events. Based on the low $\delta^{13}C$ values throughout this core, we suggest these are hyperthermals that occurred near the long-term $\delta^{13}C$ minimum preceding the Early Eocene Climate Optimum (Kirtland Turner et al., 2014). Additional, gradual variations in $\delta^{13}C$ occur between these two events without any obviously associated silicification, but these do not bear the abrupt onset or evidence for $CaCO_3$ dissolution that typically characterize hyperthermal events. Unexpectedly, $\delta^{18}O$ remains relatively invariant throughout the core, including the two intervals we interpret as early Eocene hyperthermals, which may be a result of the shallow subseafloor depth of the sediments (30–35 m) resulting in a high degree of oxygen isotopic exchange with seawater (e.g., Schrag et al., 1995).

At Site 634 in the tropical North Atlantic (Figure 6), the Paleocene-Eocene boundary was also poorly recovered, with only 30 cm of chalk overlying chert rubble recovered in the lowermost Eocene core (Austin et al., 1986). However, the immediately overlying core (634A-2R) contains nearly completely recovered white chalk of nannofossil zone NP11–NP12 (~50.4–54.1 Ma; Gradstein et al., 2012) interrupted by five discrete centimeter-scale pale yellow chert layers (Austin et al., 1986). The association between chert occurrence and negative $\delta^{13}C$ excursions at this site is less clear than at Sites U1403, U1409, 702, or 698: the upper two cherts coincide with negative $\delta^{13}C$ excursions of 0.7‰ and 0.5‰, likely hyperthermal events, while the lower three cherts do not correspond to clear CIEs. A couplet of cherts in the middle of the core

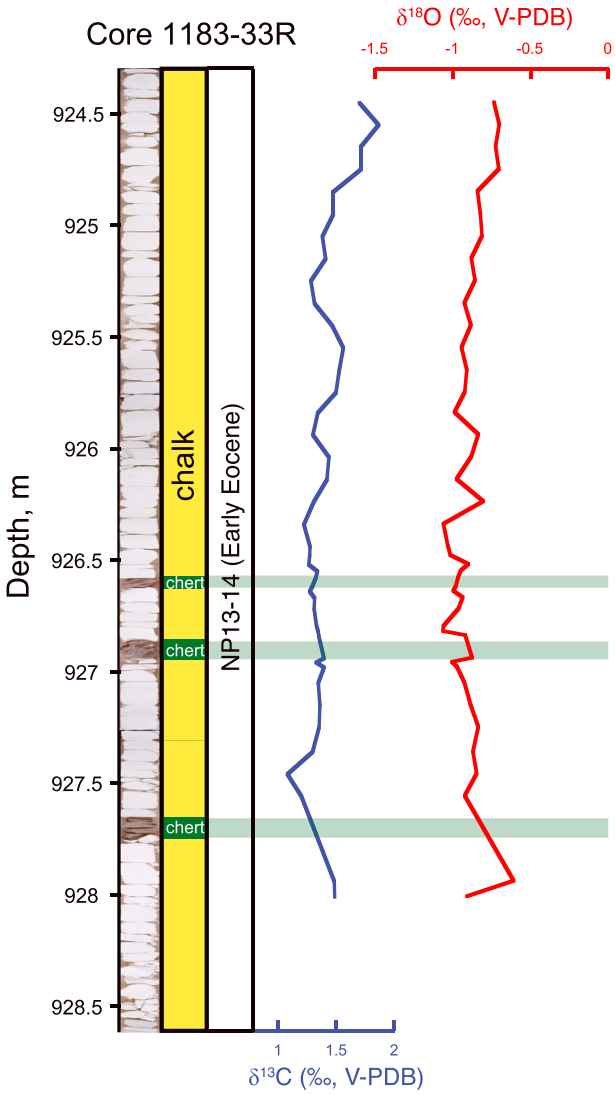

Figure 7. New records of lower Eocene siliceous sediments at Site 1183 (Ontong-Java Plateau, western Pacific). Shown are core photo, generalized lithostratigraphy, biostratigraphic constraints, and bulk carbonate stable isotope records ($\delta^{13}C_{carb}$ and $\delta^{18}O_{carb}$). V-PDB = Vienna Pee Dee Belemnite.

(centered at 148.4 m below sea floor) occurs within an interval of rapidly oscillating $\delta^{13}C$, making it difficult to diagnose potential hyperthermal events. The lowermost chert coincides with a decrease in $\delta^{13}C$ of only ~0.2‰, which falls within the background $\delta^{13}C$ variability. And, similar to Site 698, several broad excursions to lower $\delta^{13}C$ occur in the absence of any obvious silicification.

In addition to the siliceous sediments that we document as co-occurring with likely hyperthermal events, a common feature of Atlantic Deep Sea Drilling Project (DSDP) and ODP Sites is a pattern of poor core recovery of lower Eocene sediments due to a high degree of silicification. Sites 117 (Laughton & Berggren, 1972), 146, 149 (Edgar & Saunders, 1973), 390 (Party, 1978), 547 (Hinz et al., 1984), 634, 698, 961 (Mascle et al., 1996), and U1407 (Norris et al., 2014b), distributed across the Atlantic, all feature poor recovery of sediments in the lower Eocene, and particularly across the Paleocene-Eocene boundary, in some cases resulting in abandonment of the hole. Each of these sites also shows evidence that hard chert layers were the cause of the poor recovery, such as cores containing only core catchers of chert rubble or progressive silicification in overlying cores.

In the Pacific, the lower Eocene-upper Paleocene of Site 1183 (Ontong-Java Plateau, Figure 7) consists of white limestone (NP13–NP14, 47.3–50.6 Ma; Gradstein et al., 2012) interrupted by frequent centimeter-scale gray chert layers. However, $\delta^{13}C$ in our new record of lower Eocene Core 1183-33R remains nearly invariant across three of these chert layers, suggesting no association with hyperthermal events. We suggest that these chert layers may not reflect elevated silica burial at all but rather may have formed via the mechanism of Moore (2008), in which warm hydrothermal fluids dissolve biogenic silica in sediments immediately overlying basement (only ~200 m below the lower Eocene cherts in Core 1183-33R) and reprecipitate that dissolved silica as chert layers higher up in the sedimentary column. In the eastern equatorial Pacific, Sites 1220 and 1221 were investigated by Murphy et al. (2006), who found no increase in biogenic silica accumulation across the PETM.

Together, these new and published records demonstrate an association between Atlantic siliceous sediments and hyperthermal events, including the PETM. This association is particularly apparent in the middle to high latitudes of the western Atlantic, although a recent study also documents porcelainite coincident with the base of the PETM in the equatorial eastern Atlantic (Frieling et al., 2018), and a proliferation of diatoms in the earliest Eocene has also been noted in the North Sea (Mitlehner, 1996). This is consistent with a global compilation of Cenozoic chert occurrences in DSDP/ODP/IODP holes (Muttoni & Kent, 2007; Figure 1), which suggests that the Atlantic was the main locus of silica/chert deposition in the early Eocene. With the benefit of these more numerous and geospatially extensive records of hyperthermal-associated silica burial, we now revisit the hypothesis of Penman (2016) that sedimentary silica burial associated with hyperthermal events may be the result of globally elevated silicate weathering rates during such events and consider possible mechanisms for the apparent focusing of this excess silica burial into the Atlantic.

3. Numerical Modeling of the Effects of Weathering and Circulation Change on the Coupled C and Si Cycles During Hyperthermals

In order to explore the possible response of the marine silica cycle and silica burial patterns to carbon injection during Eocene hyperthermal events, we present experiments and results from LOSiCAR, a new geochemical model of the coupled carbon and silica cycles. LOSiCAR is based on the Paleogene

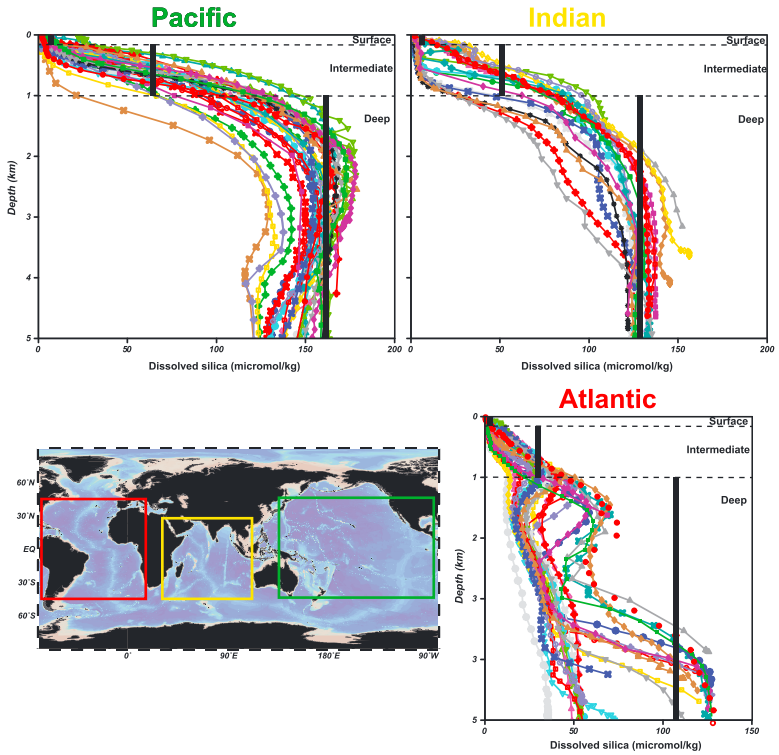

Figure 8. LOSiCAR modern steady state dissolved Si (black bars) compared to modern seawater measurements (WOCE, colored symbols—each colored symbol represents an individual location) demonstrating acceptable agreement. Complex water-mass structure in the North Atlantic (a result of local deep-water formation) cannot be resolved in LOSiCAR with a single box for the deep Atlantic. However, LOSiCAR accurately represents the large-scale patterns of $[H_4SiO_4]$ relevant to understanding the role of global circulation patterns in the silica cycle: surface depletion and deep-water enrichment, with higher $[H_4SiO_4]$ in the Pacific than in the Atlantic due to greater deep-water age. WOCE data set interrogated and plotted with Ocean Data View (Schlitzer, 2004). WOCE = World Ocean Circulation Experiment.

configuration of LOSCAR (Long-term Ocean-Sediment CArbon Reservoir model; Zeebe, 2012, v2.0.4), a numerically efficient model for long-timescale carbon cycle processes which calculates the partitioning of carbon and other relevant tracers between the atmosphere, ocean (with reservoirs representing the surface, intermediate, and deep-ocean regions of all modern ocean basins plus the Tethys), and sediments. LOSiCAR builds upon LOSCAR by implementing dissolved silica (H_4SiO_4) as an additional ocean tracer, with inventories and fluxes adopted from the two-box Si-cycle model of Penman (2016), based on estimates of modern Si cycle fluxes (Racki & Cordey, 2000; Treguer et al., 1995; Yool & Tyrrell, 2003).

In LOSiCAR, dissolved silica derived from silicate weathering (calculated using LOSCAR's parameterization of silicate weathering as a function of atmospheric pCO_2; Walker & Kasting, 1992) is delivered to each surface ocean reservoir, plus minor constant inputs of dissolved silica from hydrothermal and aeolian sources (Treguer et al., 1995; Yool & Tyrrell, 2003). The biogenic uptake of dissolved silica by opal-producing plankton in the surface ocean is modeled as a function of surface $[H_4SiO_4]$ following Penman (2016), with fixed fractions of total opal production dissolving in the surface (50%, after Yool & Tyrrell, 2005) and intermediate-depth (10%, chosen for modern data-model agreement, see below) reservoirs. The remainder is exported to the deep ocean, where some fraction of it dissolves, and the rest is buried in sediments. Partitioning between deep-ocean dissolution and burial is based on ambient deep-ocean $[H_4SiO_4]$, a dominant control on opal dissolution rates (Van Cappellen et al., 2002). A comparison of LOSiCAR's steady state dissolved silica field (modern configuration, which excludes Tethys reservoirs) with modern measurements of seawater $[H_4SiO_4]$ demonstrates acceptable large-scale agreement (Figure 8). Of course, with deep ocean basins represented by single reservoirs, LOSiCAR cannot resolve the intrabasinal structure of deep ocean geochemical gradients resulting from subbasin-scale circulation. This is particularly obvious in the

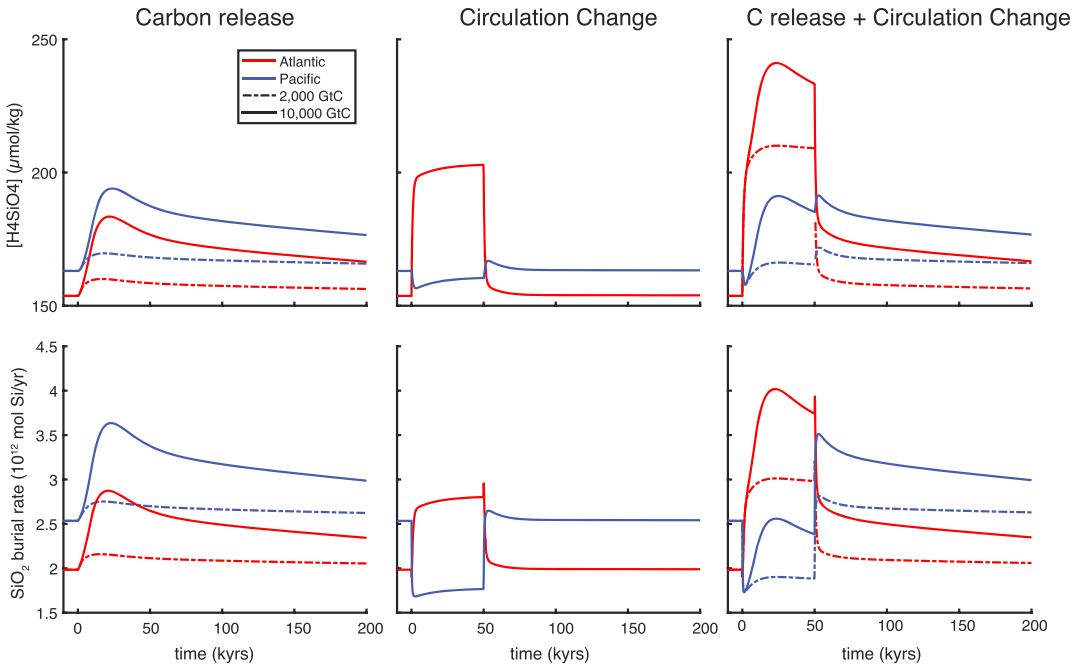

Figure 9. Results of LOSiCAR simulations of carbon release and circulation change. Top row of panels shows Atlantic (red) and Pacific (blue) deep-ocean [H_4SiO_4]; bottom panels show opal burial rate for each ocean basin. First column: Simple C release experiment, using 2,000 and 10,000 Gt C to approximately encompass the range suggested for Eocene hyperthermal events, including the Paleocene-Eocene Thermal Maximum. Second column: The circulation change of Zeebe et al. (2009), which effectively reverses the Atlantic-Pacific aging gradient and subsequently the locus of SiO_2 burial. Third column: Circulation change superimposed on the simple C release experiments in column 1.

modern deep Atlantic due to the contributions of both North Atlantic Deep Water and Antarctic Bottom Water at different depths. However, this complexity is likely not an issue in our early Eocene hyperthermal simulations, which predate modern North Atlantic Deep Water formation (Via & Thomas, 2006). Importantly, while LOSiCAR cannot resolve the local factors that control regional silica burial in the modern ocean, it does accurately represent the large-scale patterns of [H_4SiO_4] relevant to understanding the role of opal export, deep-sea dissolution, and global circulation patterns in the silica cycle. This is borne out by the model's agreement with global trends in modern marine silica cycling: surface depletion and deep-water enrichment, with higher [H_4SiO_4] (and thus SiO_2 burial) in the Pacific than the Atlantic due to greater deep-water age.

LOSiCAR offers two significant advances over the two-box model of (Penman, 2016). First, the carbon and marine silica cycles are coupled by a common silicate weathering feedback, calculated as a function of pCO_2 (Walker & Kasting, 1992), which simultaneously consumes atmospheric CO_2, restores alkalinity to the oceans (and thus restores seawater carbonate saturation following ocean acidification; Penman et al., 2016), and delivers dissolved silica to the ocean. Thus, changes in marine silica fluxes are directly tied to the modeled response to C release. Second, the differentiation of major ocean basins and parameterization of deep-ocean circulation patterns allows investigation into how changing global-scale ocean circulation could affect the spatial distribution of silica burial.

Regional differences in present-day silica burial primarily reflect upwelling intensity, as opal is undersaturated throughout the oceans and only preserved in sediments where opal production (fueled by the supply of H_4SiO_4 and other bio-limiting nutrients via the upwelling of old, deep water) outpaces dissolution in the water column and sediments, which itself is a function of deep-water [H_4SiO_4]). As a result, modern silica burial primarily occurs in the Southern Ocean and the equatorial and North Pacific Ocean. The connection between opal burial and circulation patterns is particularly important in the case of hyperthermal events because it has been argued on the basis of global ocean physics modeling (Bice & Marotzke, 2002) and spatial trends in the extent of deep-sea carbonate dissolution (Penman & Zachos, 2018; Zeebe

et al., 2009; Zeebe & Zachos, 2007) that there was a transient reversal in the deep-water aging gradient during the PETM, consistent with a switch from southern- to northern-sourced overturning. Such a large-scale circulation reversal could significantly affect regional SiO_2 burial patterns by the same mechanisms by which modern circulation focuses SiO_2 burial into the eastern equatorial Pacific and Southern Ocean.

We performed a suite of atmospheric CO_2 release and circulation change experiments using LOSiCAR (Figure 9) in which we varied the mass of carbon released from 2,000 to 10,000 Gt C to cover a range of possible C release for the PETM (e.g. Gutjahr et al., 2017; Penman & Zachos, 2018) and the smaller Eocene hyperthermals (e.g. Kirtland Turner et al., 2014; Sexton et al., 2011). These carbon release experiments were performed both with and without a prescribed circulation change as in the LOSCAR PETM simulation of (Zeebe et al., 2009), which was imposed in that study in order to reproduce the greater degree of $CaCO_3$ dissolution in the Atlantic relative to the Pacific that is apparent in sedimentary records. This circulation change consists of an overall decrease in overturning circulation strength, an increase in North Pacific deep-water (NPDW) formation, and a reduction in Southern Ocean deep-water formation. The relevant oceanographic effects of this switch include the generation of younger, less corrosive, more nutrient-poor (and in LOSiCAR, $[H_4SiO_4]$-poor) Pacific subsurface seawater and the opposite effect in the Atlantic: older, $[H_4SiO_4]$-rich subsurface seawater that upwells to fuel opal production. In our simulations, the Zeebe et al. (2009) circulation change was imposed coincident with the onset of C release for a duration of 50,000 years (approximately the length of the "body" of the PETM CIE; Rohl et al., 2007), and as a control, the same circulation change was also imposed in a simulation without any carbon release (Figure 9).

In response to simple C release experiments in LOSiCAR (Figure 9), elevated atmospheric pCO_2 immediately following C release drives elevated silicate weathering rates and dissolved silica delivery to the surface oceans, increasing seawater $[H_4SiO_4]$. This fuels greater opal production and preservation, which both lead to a subsequent increase in sedimentary opal burial. In agreement with the simple two-box model of Penman (2016), the short oceanic residence time of dissolved silica (~10,000 years) requires elevated opal burial to balance elevated riverine input relatively quickly (on timescales of 10^4 years, comparable to the duration of hyperthermal events). In the absence of circulation changes, elevated opal burial affects each ocean basin proportionally.

Changes in ocean circulation even in the absence of C release have a significant effect on LOSiCAR's patterns of opal burial (Figure 9). NPDW formation leads to lower $[H_4SiO_4]$ in the Pacific and subsequently less opal production and a smaller fraction of opal preserved in sediments. By contrast, when the Atlantic is bathed in older, $[H_4SiO_4]$-rich deep water, it upwells to fuel elevated opal production and a greater fraction is preserved in sediments. The net effect of a change in the locus of deep-water formation as in Zeebe et al. (2009) is that a nearly constant global opal burial flux is redistributed among the ocean basins, with significantly greater opal burial in the Atlantic and less in the Pacific.

When the circulation switch is imposed in combination with carbon release, as is thought to have occurred at least during the PETM and Eocene Thermal Maximum 2 (D'haenens et al., 2014), the aforementioned effects are cumulative. Immediately following C release, global opal production and burial increases in order to balance the elevated weathering flux of silica. Due to the circulation change, the majority of this elevated opal burial is focused into the Atlantic, which exhibits a 100–200% increase in opal burial rate depending on the size of C release. In the Pacific, the effects of circulation change (which tends to reduce opal burial) is approximately balanced by the effects of elevated weathering flux (which tends to increase burial), leading to approximately unchanged Pacific opal burial rates with a large C release (10,000 Gt C). In the case of the small C release (2,000 Gt C), the effects of circulation change dominate and there is a net decrease in Pacific opal burial. Rapid fluctuations in Pacific opal burial rate at the onset and cessation of the circulation forcing reflect the different response timescales of the two forcings (the circulation change immediately affects $[H_4SiO_4]$ distribution, while the enhanced weathering take 10^3–10^4 years to appreciably increase silica supply). However, the timescale of the Si burial response to circulation change is controlled by the instantaneous onset and cessation of NPDW formation applied in the model, whereas it might be expected to have occurred more gradually during hyperthermal recoveries.

4. Conclusions

Our new records of hyperthermal-associated siliceous sedimentation demonstrate that the elevated silica burial in the North Atlantic during the PETM documented by Penman (2016) was not restricted to the North Atlantic, nor was it a unique feature of the PETM alone. The similar sedimentary character of the PETM in the North and South Atlantic suggests that elevated silica burial during that event extended throughout the Atlantic basin. Furthermore, the association of cherts with later hyperthermal events at Sites U1409, 698, and 634 suggests that elevated silica burial was a common feature of Eocene hyperthermal events, at least in parts of the North and South Atlantic. Of course, not all cherts of Eocene age can be assigned unambiguously to hyperthermal events (e.g., Site 634 contains lower Eocene cherts without any obvious CIE), and only a small subset of existing records of hyperthermal events show evidence for enhanced silica burial, even within the Atlantic (e.g., Zachos et al., 2005). But the previously unknown co-occurrence of cherts with $\delta^{13}C$ excursions in both the North and South Atlantic across the PETM and later hyperthermal events suggests a common formation mechanism.

Our LOSiCAR simulations support the previous assertion (Penman, 2016) that if silicate weathering is key to the recovery from carbon release events like the PETM, then an inevitable implication is significantly elevated riverine input of dissolved silica to the oceans, resulting in profound changes in the marine silica cycle including a prompt increase in silica burial rates. By concentrating old, $[H_4SiO_4]$-rich water that upwells to fuel local opal production, changes in circulation can explain the focusing of this excess silica burial into the Atlantic. Our results thus indirectly suggest that changes in the locus of deep-water formation may have occurred across multiple early Eocene hyperthermals. This mechanism, recurring during dozens of individual hyperthermal events, may at least in part explain the preponderance of lower Eocene chert in the Atlantic relative to other basins and time periods (Figure 1). More records, especially from upwelling regions outside the Atlantic, are needed to fully constrain the spatial distribution of silica burial during hyperthermal events. Regardless, the global reorganization of deep-ocean circulation patterns like that proposed for the PETM may be of comparable or greater importance than enhanced weathering response alone, especially when considering individual records of local silica burial across abrupt warming events. The mechanisms explored here help shed light on the curious case of Atlantic Eocene cherts and may be important in interpreting cherts and other siliceous facies in other periods of Earth's history.

Acknowledgments
We thank IODP, its core repositories, and legacy programs for access to core material and initial descriptions, Brad Erkkila and Marvin Wint for assistance at the Yale Analytical and Stable Isotope Center, Richard Zeebe for guidance with adding dissolved silica to his LOSCAR model, and two anonymous reviewers for constructive suggestions. D. E. P. is supported by Yale's Flint postdoctoral fellowship and funding from IODP and NSF, and S. D. and P. M. H. by NSF OCE 1536604. XRF Si intensity data and bulk carbonate stable isotope data are available as online supporting information associated with this article.

References

Alley, R. B. (2016). A heated mirror for future climate. *Science*, *352*(6282), 151–152. https://doi.org/10.1126/science.aaf4837

Austin, J., Schlager, W., & Palmer, A. (1986). *Leg 101: Proceedings initial reports (Pt. A)*. College Station, TX: Ocean Drilling Program.

Babila, T., Penman, D., Hönisch, B., Kelly, D., Bralower, T., Rosenthal, Y., & Zachos, J. (2018). Capturing the global signature of surface ocean acidification during the Palaeocene-Eocene Thermal Maximum. *Philosophical Transactions Series A, Mathematical, Physical, and Engineering Sciences*, *376*(2130), 20170072. https://doi.org/10.1098/rsta.2017.0072

Berner, R. A., Lasaga, A. C., & Garrels, R. M. (1983). The carbonate-silicate geochemical cycle and its effects on atmospheric carbon dioxide over the past 100 million years. *American Journal of Science*, *283*(7), 641–683. https://doi.org/10.2475/ajs.283.7.641

Bice, K. L., & Marotzke, J. (2002). Could changing ocean circulation have destabilized methane hydrate at the Paleocene-Eocene boundary? *Paleoceanography*, *17*(2), 1018. https://doi.org/10.1029/2001PA000678

Calvert, S. (1971). Composition and origin of North Atlantic deep sea cherts. *Contributions to Mineralogy and Petrology*, *33*(4), 273–288. https://doi.org/10.1007/BF00382569

Ciesielski, P., & Kristoffersen, Y. (1988). Leg 114. In *Proceedings of the ODPInitial Reports* (Vol. 114, p. 815). College Station, TX: Ocean Drilling Program.

D'haenens, S., Bornemann, A., Claeys, P., Roehl, U., Steurbaut, E., & Speijer, R. P. (2014). A transient deep-sea circulation switch during Eocene Thermal Maximum 2. *Paleoceanography*, *29*, 370–388. https://doi.org/10.1002/2013PA002567

Dickens, G. R., Castillo, M. M., & Walker, J. C. G. (1997). A blast of gas in the latest Paleocene: Simulating first-order effects of massive dissociation of oceanic methane hydrate. *Geology*, *25*(3), 259–262. https://doi.org/10.1130/0091-7613(1997)025<0259:ABOGIT>2.3.CO;2

Dickson, A. J., Cohen, A. S., Coe, A. L., Davies, M., Shcherbinina, E. A., & Gavrilov, Y. O. (2015). Evidence for weathering and volcanism during the PETM from Arctic Ocean and Peri-Tethys osmium isotope records. *Palaeogeography, Palaeoclimatology, Palaeoecology*, *438*, 300–307. https://doi.org/10.1016/j.palaeo.2015.08.019

Dunkley-Jones, T., Lunt, D. J., Schmidt, D. N., Ridgwell, A., Sluijs, A., Valdes, P. J., & Maslin, M. (2013). Climate model and proxy data constraints on ocean warming across the Paleocene–Eocene Thermal Maximum. *Earth-Science Reviews*, *125*, 123–145. https://doi.org/10.1016/j.earscirev.2013.07.004

Edgar, N., & Saunders, J. (Eds.) (1973). *Initial reports of the Deep Sea Drilling Project* (Vol. 15, pp. 17–168). Washington, DC: U. S Government Printing Office.

Frieling, J., Reichart, G.-J., Middelburg, J. J., Röhl, U., Westerhold, T., Bohaty, S. M., & Sluijs, A. (2018). Tropical Atlantic climate and ecosystem regime shifts during the Paleocene–Eocene Thermal Maximum. *Climate of the Past*, *14*, 39–55. https://doi.org/10.5194/cp-14-39-2018

Gibson, T. G., & Towe, K. M. (1971). Eocene volcanism and the origin of Horizon A. *Science*, *172*(3979), 152–154. https://doi.org/10.1126/science.172.3979.152

Gradstein, F. M., Ogg, J. G., Schmitz, M., & Ogg, G. (2012). *The geologic time scale 2012*. New York: Elsevier.

Gutjahr, M., Ridgwell, A., Sexton, P. F., Anagnostou, E., Pearson, P. N., Pälike, H., et al. (2017). Very large release of mostly volcanic carbon during the Palaeocene–Eocene Thermal Maximum. *Nature*, *548*(7669), 573.

Hesse, R. (1988). Diagenesis# 13. Origin of chert: Diagenesis of biogenic siliceous sediments. *Geoscience Canada*, *15*(3).

Hinz, K., Winterer, E., Baumgartner, P., Bradshaw, M., Channell, J., Jansa, L., et al. (1984). Initial reports of the Deep-Sea Drilling Project. In *Covering leg-79 of the cruises of the drilling vessel Glomar-Challenger Las-Palmas, Grand-Canary-Island, to Brest, France April May 1981-site-547* (Vol. 79, pp. 223–361).

Katz, M., & Miller, K. G. (1991). Early Paleogene benthic foraminiferal assemblages and stable isotopes in the Southern Ocean. In P. F. Ciesielski et al. (Eds.), *Proceedings of the Ocean Drilling Program, scientific results* (Vol. 114, pp. 481–513). College Station, TX: Ocean Drilling Program.

Kelly, D. C., Nielsen, T. M. J., McCarren, H. K., Zachos, J. C., & Rohl, U. (2010). Spatiotemporal patterns of carbonate sedimentation in the South Atlantic: Implications for carbon cycling during the Paleocene-Eocene Thermal Maximum. *Palaeogeography Palaeoclimatology Palaeoecology*, *293*(1–2), 30–40. https://doi.org/10.1016/j.palaeo.2010.04.027

Kennett, J. P., & Stott, L. D. (1991). Abrupt deep-sea warming, palaeoceanographic changes and benthic extinctions at the end of the Palaeocene. *Nature*, *353*(6341), 225–229. https://doi.org/10.1038/353225a0

Kirtland Turner, S., Sexton, P. F., Charles, C. D., & Norris, R. D. (2014). Persistence of carbon release events through the peak of early Eocene global warmth. *Nature Geoscience*, *7*(10), 748–751. https://doi.org/10.1038/ngeo2240

Knauth, L. P. (1979). A model for the origin of chert in limestone. *Geology*, *7*(6), 274–277. https://doi.org/10.1130/0091-7613(1979)7<274:AMFTOO>2.0.CO;2

Koch, P. L., Zachos, J. C., & Gingerich, P. D. (1992). Correlation between isotope records in marine and continental carbon reservoirs near the Palaeocene Eocene boundary. *Nature*, *358*(6384), 319–322. https://doi.org/10.1038/358319a0

Laschet, C. (1984). On the origin of cherts. *Facies*, *10*(1), 257–289. https://doi.org/10.1007/BF02536693

Laughton, A., & Berggren, W. (1972). Sites 116 and 117. In *Initial reports Deep Sea Drilling Project* (Vol. 12, pp. 395–671). College Station, TX: Deep Sea Drilling Program.

Littler, K., Röhl, U., Westerhold, T., & Zachos, J. C. (2014). A high-resolution benthic stable-isotope record for the South Atlantic: Implications for orbital-scale changes in late Paleocene–early Eocene climate and carbon cycling. *Earth and Planetary Science Letters*, *401*, 18–30. https://doi.org/10.1016/j.epsl.2014.05.054

Mascle, J., Lohmann, G., & Clift, P. (1996). Principal results. In *Proceedings of the Ocean Drilling Program, initial reports* (Vol. 159, pp. 297–314). College Station, TX: Ocean Drilling Program.

McGowran, B. (1989). Silica burp in the Eocene ocean. *Geology*, *17*(9), 857–860. https://doi.org/10.1130/0091-7613(1989)017<0857:SBITEO>2.3.CO;2

McInerney, F. A., & Wing, S. L. (2011). The Paleocene-Eocene Thermal Maximum: A perturbation of carbon cycle, climate, and biosphere with implications for the future. *Annual Review of Earth and Planetary Sciences*, *39*(1), 489–516. https://doi.org/10.1146/annurev-earth-040610-133431

Mitlehner, A. G. (1996). Palaeoenvironments in the North Sea basin around the Paleocene-Eocene boundary: Evidence from diatoms and other siliceous microfossils. *Geological Society, London, Special Publications*, *101*(1), 255–273. https://doi.org/10.1144/GSL.SP.1996.101.01.15

Moore, T. (2008). Chert in the Pacific: Biogenic silica and hydrothermal circulation. *Palaeogeography, Palaeoclimatology, Palaeoecology*, *261*(1-2), 87–99. https://doi.org/10.1016/j.palaeo.2008.01.009

Murphy, B., Lyle, M., & Olivarez Lyle, A. (2006). Biogenic burial across the Paleocene/Eocene boundary: Ocean Drilling Program Leg 199 Site 1221. In P. A. Wilson, M. Lyle, & J. V. Firth (Eds.), *Proc. ODP, Sci. Results* (Vol. 199, pp. 1–12). College Station, TX: Ocean Drilling Project.

Muttoni, G., & Kent, D. V. (2007). Widespread formation of cherts during the early Eocene climate optimum. *Palaeogeography, Palaeoclimatology, Palaeoecology*, *253*(3-4), 348–362. https://doi.org/10.1016/j.palaeo.2007.06.008

Norris, R., Wilson, P., Blum, P., Fehr, A., Agnini, C., Bornemann, A., et al. (2014a). Site U1409. In *Proceedings of the Integrated Ocean Drilling Program* (Vol. 342, pp. 1–104). College Station, TX: Integrated Ocean Drilling Program. https://doi.org/10.2204/iodp.proc.342.110.2014

Norris, R., Wilson, P., Blum, P., Fehr, A., Agnini, C., Bornemann, A., et al. (2014b). Site U1407. In R. D. Norris, P. A. Wilson, P. Blum, & Expedition, 342 Scientists (Eds.), *Proc. IODP* (Vol. 342, pp. 1–106). College Station, TX: Integrated Ocean Drilling Program.

Panchuk, K., Ridgwell, A., & Kump, L. R. (2008). Sedimentary response to Paleocene-Eocene Thermal Maximum carbon release: A model-data comparison. *Geology*, *36*(4), 315–318. https://doi.org/10.1130/G24474A.1

Party, S. S. (1978). Sites 389 and 390: North rim of Blake Nose. *Initial Reports of the Deep Sea Drilling Project*, *44*, 69–151.

Penman, D. E. (2016). Silicate weathering and North Atlantic silica burial during the Paleocene-Eocene Thermal Maximum. *Geology*, *44*(9), 731–734. https://doi.org/10.1130/G37704.1

Penman, D. E., Hönisch, B., Zeebe, R. E., Thomas, E., & Zachos, J. C. (2014). Rapid and sustained surface ocean acidification during the Paleocene-Eocene Thermal Maximum. *Paleoceanography*, *29*, 357–369. https://doi.org/10.1002/2014PA002621

Penman, D. E., Turner, S. K., Sexton, P. F., Norris, R. D., Dickson, A. J., Boulila, S., et al. (2016). An abyssal carbonate compensation depth overshoot in the aftermath of the Palaeocene-Eocene Thermal Maximum. *Nature Geoscience*, *9*, 575–580. https://doi.org/10.1038/ngeo2757

Penman, D. E., & Zachos, J. C. (2018). New constraints on massive carbon release and recovery processes during the Paleocene-Eocene Thermal Maximum. *Environmental Research Letters*, *13*(10). https://doi.org/10.1088/1748-9326/aae285

Racki, G., & Cordey, F. (2000). Radiolarian palaeoecology and radiolarites: Is the present the key to the past? *Earth-Science Reviews*, *52*(1-3), 83–120. https://doi.org/10.1016/S0012-8252(00)00024-6

Ravizza, G., Norris, R., Blusztajn, J., & Aubry, M. P. (2001). An osmium isotope excursion associated with the late Paleocene Thermal Maximum: Evidence of intensified chemical weathering. *Paleoceanography*, *16*(2), 155–163.

Rohl, U., Westerhold, T., Bralower, T. J., & Zachos, J. C. (2007). On the duration of the Paleocene-Eocene Thermal Maximum (PETM). *Geochemistry, Geophysics, Geosystems*, *8*, Q12002. https://doi.org/10.1029/2007GC001784

Schlitzer, R. (2004). Ocean Data View.

Schrag, D. P., DePaolo, D. J., & Richter, F. M. (1995). Reconstructing past sea surface temperatures: Correcting for diagenesis of bulk marine carbonate. *Geochimica et Cosmochimica Acta*, *59*(11), 2265–2278. https://doi.org/10.1016/0016-7037(95)00105-9

Sexton, P. F., Norris, R. D., Wilson, P. A., Pälike, H., Westerhold, T., Röhl, U., et al. (2011). Eocene global warming events driven by ventilation of oceanic dissolved organic carbon. *Nature*, *471*(7338), 349.

Treguer, P., Nelson, D. M., Van Bennekom, A. J., DeMaster, D. J., Leynaert, A., & Quéguiner, B. (1995). The silica balance in the world ocean: A reestimate. *Science*, *268*(5209), 375–379. https://doi.org/10.1126/science.268.5209.375

Van Cappellen, P., Dixit, S., & van Beusekom, J. (2002). Biogenic silica dissolution in the oceans: Reconciling experimental and field-based dissolution rates. *Global Biogeochemical Cycles*, *16*(4), 1075. https://doi.org/10.1029/2001GB001431

Via, R. K., & Thomas, D. J. (2006). Evolution of Atlantic thermohaline circulation: Early Oligocene onset of deep-water production in the North Atlantic. *Geology*, *34*(6), 441–444. https://doi.org/10.1130/G22545.1

Walker, J. C. G., Hays, P. B., & Kasting, J. F. (1981). A negative feedback mechanism for the long-term stabilization of Earth's surface-temperature. *Journal of Geophysical Research*, *86*(Nc10), 9776–9782.

Walker, J. C. G., & Kasting, J. F. (1992). Effects of fuel and forest conservation on future levels of atmospheric carbon dioxide. *Palaeogeography Palaeoclimatology Palaeoecology*, *97*(3), 151–189. https://doi.org/10.1016/0031-0182(92)90207-L

Westerhold, T., Röhl, U., Donner, B., & Zachos, J. (2018). Global extent of early Eocene hyperthermal events—A new Pacific benthic foraminiferal isotope record from Shatsky Rise (ODP Site 1209). *Paleoceanography and Paleoclimatology*, *33*, 626–642. https://doi.org/10.1029/2017PA003306

Yool, A., & Tyrrell, T. (2003). Role of diatoms in regulating the ocean's silicon cycle. *Global Biogeochemical Cycles*, *17*(4), 1103. https://doi.org/10.1029/2002GB002018

Yool, A., & Tyrrell, T. (2005). Implications for the history of Cenozoic opal deposition from a quantitative model. *Palaeogeography, Palaeoclimatology, Palaeoecology*, *218*(3-4), 239–255. https://doi.org/10.1016/j.palaeo.2004.12.017

Zachos, J. C., McCarren, H., Murphy, B., Röhl, U., & Westerhold, T. (2010). Tempo and scale of late Paleocene and early Eocene carbon isotope cycles: Implications for the origin of hyperthermals. *Earth and Planetary Science Letters*, *299*(1-2), 242–249. https://doi.org/10.1016/j.epsl.2010.09.004

Zachos, J. C., Rohl, U., Schellenberg, S. A., Sluijs, A., Hodell, D. A., Kelly, D. C., et al. (2005). Rapid acidification of the ocean during the Paleocene-Eocene Thermal Maximum. *Science*, *308*(5728), 1611–1615.

Zachos, J. C., Wara, M. W., Bohaty, S., Delaney, M. L., Petrizzo, M. R., Brill, A., et al. (2003). A transient rise in tropical sea surface temperature during the Paleocene-Eocene Thermal Maximum. *Science*, *302*(5650), 1551–1554.

Zeebe, R. (2012). LOSCAR: Long-term Ocean-atmosphere Sediment CArbon Reservoir model v2.0.4. *Geoscientific Model Development*, *5*, 149–166.

Zeebe, R. E., & Zachos, J. C. (2007). Reversed deep-sea carbonate ion basin gradient during Paleocene-Eocene Thermal Maximum. *Paleoceanography*, *22*, PA3201. https://doi.org/10.1029/2006PA001395

Zeebe, R. E., Zachos, J. C., & Dickens, G. R. (2009). Carbon dioxide forcing alone insufficient to explain Palaeocene-Eocene Thermal Maximum warming. *Nature Geoscience*, *2*(8), 576–580. https://doi.org/10.1038/ngeo578